Imprint of electron returning dynamics on ion momentum spectra in strong-field nonsequential double ionization

Tongtong He,[1] Zichao Liu,[1] Jianying Liao,[1] Yingbin Li,[2] Benhai Yu,[2] and Cheng Huang[1,*]

[1]*School of Physical Science and Technology and Chongqing Key Laboratory of Micro & Nano Structure Optoelectronics, Southwest University, Chongqing 400715, China*

[2]*College of Physics and Electronic Engineering, Xinyang Normal University, Xinyang 464000, China*

(Received 29 November 2023; revised 27 January 2024; accepted 19 March 2024; published 10 April 2024)

Nonsequential double ionization (NSDI) of atoms driven by parallel-polarized two-color (PPTC) fields composed of two equal-intensity multiple-cycle laser pulses is investigated using a three-dimensional classical ensemble model. The ion momentum distribution shows pronounced asymmetry and strongly depends on the relative phase of the two pulses. The ion momentum distributions exhibit a double- or not yet observed triple-hump structure, depending on the relative phase of the two pulses. More interestingly, the three peaks of the ion momentum distribution correspond to the first-returning recollision, the odd-returning recollision (without the first returning recollision), and the even-returning recollision. This means that the number of electron returnings is mapped onto the ion momentum distribution. The information about the number of electron returnings can be directly retrieved from the observed ion momentum distribution in the PPTC field with equal intensities. Moreover, the proportions of the three types of trajectories in NSDI, the returning energy of the ionized electron, and the ionization mechanism can be well manipulated by changing the relative phase of the two pulses.

DOI: 10.1103/PhysRevA.109.043109

I. INTRODUCTION

With the rapid development of ultrafast laser technology, many novel high-order nonlinear phenomena have been observed in the interactions of intense laser fields with atoms and molecules, such as high-order harmonic generation (HHG), above-threshold ionization (ATI), nonsequential double ionization (NSDI) [1,2], etc. Strong-field NSDI involves the correlated dynamics of two electrons and has been one of the hot topics in the study of strong-field physics in the past few decades [3–15]. NSDI can be well described by the quasiclassical recollision model [16,17]. First, an electron in an atom escapes from the nucleus driven by a strong laser electric field. When the laser field is reversed, the ionized electron is pulled back to the nucleus and collides with it inelastically. After the recollision, a second electron may be ionized directly [5,18] or excited and then ionized by the subsequent laser field with a time delay [18–21].

In a multiple-cycle linear laser pulse, the ionized electron can return and collide with the parent ion from the left and right directions with the same probability. Therefore, the ion momentum spectra and correlated electron momentum spectra from NSDI show a symmetric distribution [3–7]. The laser intensity and wavelength can significantly affect the returning energy and the transversal distance when the ionized electron returns to the parent ion and can further affect the efficiency of energy transfer between the two electrons and the NSDI mechanism [22–33]. For a few-cycle laser pulse with a stabilized carrier-envelope phase (CEP), the left-right symmetry of the laser electric-field wave form is broken. The returning probability and energy of the ionized electron from the left and right directions are very different. The ion and correlated electron momentum spectra exhibit significant asymmetry. The CEP of the few-cycle laser pulse determines the wave form of the electric field and can control the recollision dynamics and the correlation behavior of the two electrons [34–37]. Compared with a single CEP-stabilized few-cycle pulse, the combined electric field composed of two linearly polarized pulses with different frequencies is also asymmetric, and its wave form can be more flexibly controlled by changing the relative intensity and phase between the two pulses. Therefore, parallel-polarized two-color (PPTC) fields are widely used to control HHG and ATI [38–41].

In 2010, Zhou *et al.* used the few-cycle PPTC laser fields to induce NSDI [42]. By controlling the relative phase between the two pulses, the recollision of the ionized electron can be controlled within a time interval of several hundred attoseconds, thus showing an arclike structure on the correlated electron momentum distribution. Then Ma *et al.* theoretically studied the correlated electron dynamics in a multicycle PPTC field [43]. The results show that the recollision energy can be accurately controlled with the PPTC field. The ion momentum distributions in the direction parallel to the polarization of the laser field exhibit a single- or double-hump structure, depending on the relative phase of the two pulses. Subsequently, Luo *et al.* experimentally measured the momentum distribution of Ne^{2+} from NSDI using a multicycle PPTC field consisting of a strong 800-nm field and a weak 400-nm field [44]. The ion momentum distribution measured by experiment

*huangcheng@swu.edu.cn

 ©2024 American Physical Society

shows pronounced asymmetry in the emission direction. The peak of the ion momentum distribution shifts gradually with the relative phase, which is attributed to the change in the recollision time with the relative phase of the two pulses. All of the above studies on NSDI of atoms driven by PPTC fields used the combination of a strong driving laser field and a very weak controlling laser field. It can be expected that when the two pulses have comparable intensities, the wave form of the combined electric field will be more complex, and NSDI will exhibit richer electron correlated dynamics, where the single ionization, the returning and collision process, the electron correlation behavior, and their dependence on the relative phase of the two pulses will be very different and more complex compared to the PPTC field with two significantly different intensities employed in previous works. In this paper, we investigate NSDI of atoms driven by PPTC fields composed of two equal-intensity multiple-cycle laser pulses. The ion momentum distribution shows pronounced asymmetry and strongly depends on the relative phase of the two pulses. The ion momentum distributions exhibit a double- or not yet observed three-hump structure, depending on the relative phase of the two-color fields. Moreover, different from those previous works using a PPTC field with two significantly different intensities, where the recollision occurs at the first returning of the free electron, in the PPTC field with two equal intensities many free electrons miss the parent ion because of the transverse distance when they return to the parent ion for the first time in the longitudinal direction, and the effective recollision occurs after several returns. These multiple-returning recollision trajectories make a considerable contribution to NSDI, and its proportion in NSDI depends on the relative phase of the two pulses. More interestingly, the three peaks of the ion momentum distribution correspond to the first-returning recollision, the odd-returning recollision (without the first-returning recollision), and the even-returning recollision. This means that the number of electron returnings is mapped onto the ion momentum spectrum, and thus, the electron returning dynamics for different peaks in the ion momentum distributions can be directly determined in the PPTC fields.

II. METHODS

In this paper, we use the three-dimensional classical ensemble model developed by Haan *et al.* to study NSDI of He in PPTC laser fields [45]. It has been proved that the classical model is very successful in interpreting and predicting NSDI phenomena [8,9,46–48]. In the model, the nucleus is fixed at the origin, and the motion of the two electrons follows the classical Newtonian equations (atomic units are used throughout unless stated otherwise):

$$\frac{d^2\mathbf{r}_i}{dt^2} = -\nabla[V_{ne}(\mathbf{r}_i) + V_{ee}(\mathbf{r}_1, \mathbf{r}_2)] - \mathbf{E}(t), \qquad (1)$$

where $\mathbf{r}_1$ and $\mathbf{r}_2$ are the position vectors of the two electrons. $V_{ne}(\mathbf{r_i}) = -\frac{2}{\sqrt{\mathbf{r_i}^2+a}}$ represents the Coulomb potential energy between the electron and the nucleus. $V_{ee}(\mathbf{r}_1, \mathbf{r}_2) = \frac{1}{\sqrt{(\mathbf{r}_1-\mathbf{r}_2)^2+b}}$ represents the Coulomb potential energy between the two electrons. The softening parameters $a = 0.75$ and $b = 0.01$ are introduced to avoid autoionization and guarantee numerical stability. $\mathbf{E}(t)$ is the combined electric field consisting of two laser pulses. It is written as $\mathbf{E}(t) = f(t)E_0[\sin(\omega t)\hat{z} + \sin(2\omega t + \phi)\hat{z}]$. In this work the wavelengths of the two linearly polarized pulses are 1600 and 800 nm. Their angular frequencies are denoted ω and 2ω. E_0 is the electric-field amplitude. The corresponding laser intensity is 2×10^{14} W/cm^2. ϕ is the relative phase between the 800- and 1600-nm laser fields. The period of the 1600-nm laser pulse is labeled T. $f(t)$ is the trapezoidal pulse envelope with $2T$ on and off ramps and an $8T$ platform interval.

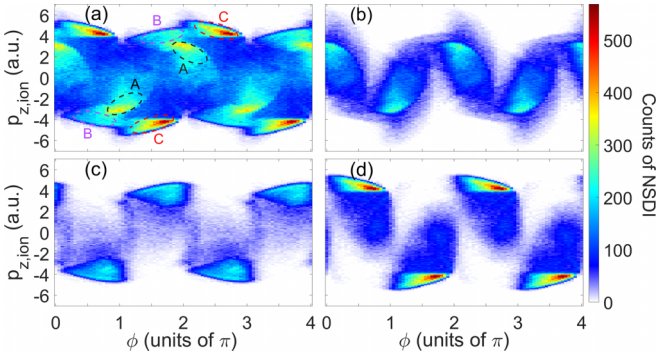

FIG. 1. The ion momentum distribution along the laser polarization direction vs the relative phase between two pulses. (a) All double-ionization events, (b) FRR double-ionization events, (c) ORR double-ionization events without those FRR events, and (d) ERR double-ionization events.

To obtain a stable initial ensemble, we first place two electrons randomly near the nucleus. Then we can calculate the potential energy of the two-electron system for the given positions $E_p = V_{ne}(\mathbf{r}_1) + V_{ne}(\mathbf{r}_2) + V_{ee}(\mathbf{r}_1, \mathbf{r}_2)$. The total energy $E_{\text{total}} = -2.9035$ a.u. is the ground-state energy of the He atom. The sum of the kinetic energies of the two electrons equals $E_{\text{total}} - E_p$. After ensuring $E_k > 0$ for the given positions, we randomly assign the kinetic energy between the two electrons, and the directions of momenta for the two electrons are randomly determined. Then the two electrons are evolved freely for a sufficiently long time (150 a.u.) without the laser electric field until a stable initial ensemble is obtained. Subsequently, the laser electric field is turned on, and these trajectories evolve in the electric and Coulomb fields until the laser pulse ends. If the final energies of both electrons in an atom are greater than zero, double ionization occurs. In this work, for each relative phase, 15 000 double-ionization events are obtained. Depending on the relative phase, the ensemble size ranges from 6 to 10 million.

III. RESULTS AND DISCUSSION

Figure 1(a) shows the ion momentum distribution along the laser polarization direction vs the relative phase between the two pulses. The ion momenta are obtained with $\mathbf{p}_{\text{He}^{2+}} = -(\mathbf{p}_{e1} + \mathbf{p}_{e2})$. It is obvious that the ion momentum distributions are asymmetric in the emission direction and strongly depend on the relative phase between the two pulses. This is because the wave form of the combined electric field is asymmetric for the positive and negative parts and varies

with the relative phase. More interestingly, the ion momentum distribution in the positive or negative direction consists of three parts, which are marked by ellipses A, B, and C. With the variation of the relative phase between the two pulses, the ion momentum distributions exhibit a double- or triple-hump structure, which is significantly different from the results for the combination of a strong driving field and a very weak controlling field. In previous studies on PPTC fields composed of a strong driving field and a weak controlling field, the ions in the positive or negative direction mainly gather in a region, and the ion momentum distributions show the single- or double-hump structure [43,44], depending on the relative phase of the two-color fields.

To clarify why the ion momentum distribution along the laser polarization direction exhibits a particular structure, we trace those NSDI trajectories and find that for some NSDI events the first ionized electron from the atom recollides with the parent ion and transfers part of the energy to the second electron, leading to double ionization when it returns to the vicinity of the parent ion the first time, whereas for many other NSDI events the free electron misses the parent ion because of the transverse distance when it returns to the parent ion the first time in the longitudinal direction. For these trajectories no energy exchange (recollision) occurs at the first returning of the free electron in the longitudinal direction. Then, the free electron continues oscillating by the laser electric field. After several returns in the longitudinal direction, due to the Coulomb focusing effect of the parent ion in the transverse direction, the free electron can recollide with the parent ion and release the other bound electron. The process is different from those in previous studies on NSDI using the PPTC field with two significantly different intensity pulses, where the recollision occurs during the first returning of the free electron [42–44]. Moreover, in the calculation, by tracing NSDI trajectories we can obtain the returning number of the free electron for each trajectory from single ionization to recollision. The counting rule is that whenever the free electron passes through the plane $z = 0$ (the laser polarization direction is along the z axis), the returning number is increased by 1 until recollision, which is recorded as the last returning. Trajectory analysis shows that the final ion momentum distribution is closely related to the returning number of the free electron before recollision.

Based on the returning number of the free electron, those NSDI trajectories are classified into three types: the first-returning-recollision (FRR) trajectory, the odd-returning-recollision (ORR) trajectory without the FRR, and the even-returning-recollision (ERR) trajectory. Figures 1(b)–1(d) show the ion momentum distributions along the laser polarization direction for FRR events, ORR events without the FRR, and ERR events, respectively, which correspond well to regions A, B, and C in the total distribution in Fig. 1(a). The ion momentum distribution caused by each type of trajectory has its own particular shape, and each type is located in a different region. We can also see that the ion momentum caused by the ERR is generally greater than that caused by the FRR. This means that the information about the returning number of the free electron is encoded in the ion momentum distribution. One can directly retrieve the electron returning number from the observed ion momentum distribution. Depending on the

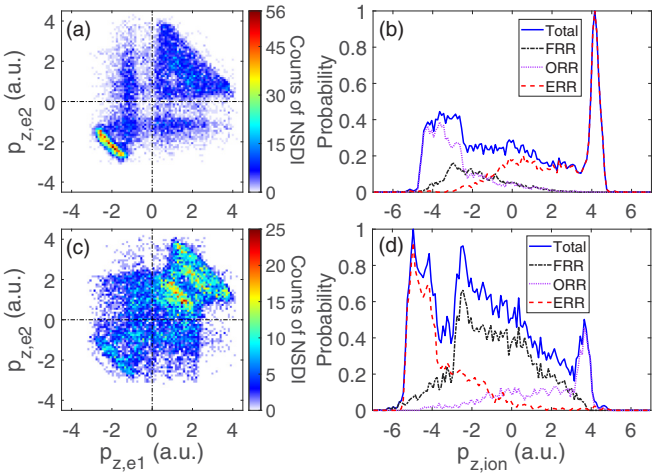

FIG. 2. Correlated (a) and (c)electron momentum distributions and (b) and (d) ion momentum distributions along the laser polarization direction for relative phases of (a) and (b) 0.75π and (c) and (d) 1.25π. Solid blue curve: all events; dash-dotted black curve: FRR events; dotted purple curve: ORR events without the FRR; and dashed red curve: ERR events. The maximum value in (b) and (d) has been normalized to 1.

relative phases of the two pulses, the relative contributions from the three types of trajectories are quite different, and the ion momentum distributions exhibit a double- or triple-hump structure. For example, for $\phi = 0.75\pi$ the NSDI mainly proceeds by ORR trajectories without the FRR and ERR trajectories; therefore, the ion momentum distribution shows a double-hump structure. For $\phi = 1.25\pi$ all three types of trajectories make considerable contributions to NSDI, and therefore, three peaks can be observed in the ion momentum distribution [see Fig. 1(a)].

To more clearly reveal the underlying ultrafast dynamics responsible for the evolution of the ion momentum distribution with the relative phase of the two pulses, we analyze the correlated electron momentum distribution, ion momentum distribution, single-ionization time, recollision time, and double-ionization time for the three types of trajectories. Figure 2 shows the correlated electron momentum distributions [Figs. 2(a) and 2(c)] and ion momentum distributions [Figs. 2(b) and 2(d)] along the laser polarization direction for two typical relative phases: 0.75π [Figs. 2(a) and 2(b)] and 1.25π [Figs. 2(c) and 2(d)]. Figure 3 shows the time distributions of the single ionization (left column), recollision (middle column), and double ionization (right column) for the 0.75π (top row) and 1.25π (bottom row) relative phases. Here, the single-ionization time is defined as the instant when one electron is outside the nuclear well. The double-ionization time is defined as the instant when both electrons achieve positive energies. The recollision time is defined as the instant of the closest approach after the first departure of one electron from the parent ion.

For $\phi = 0.75\pi$, the electron pairs mainly distribute in the first and third quadrants, as shown in Fig. 2(a), indicating that the correlated emission is dominant. The total ion momentum spectrum shows a double-hump structure [see the solid blue curve in Fig. 2(b)]. In this phase, the proportion of

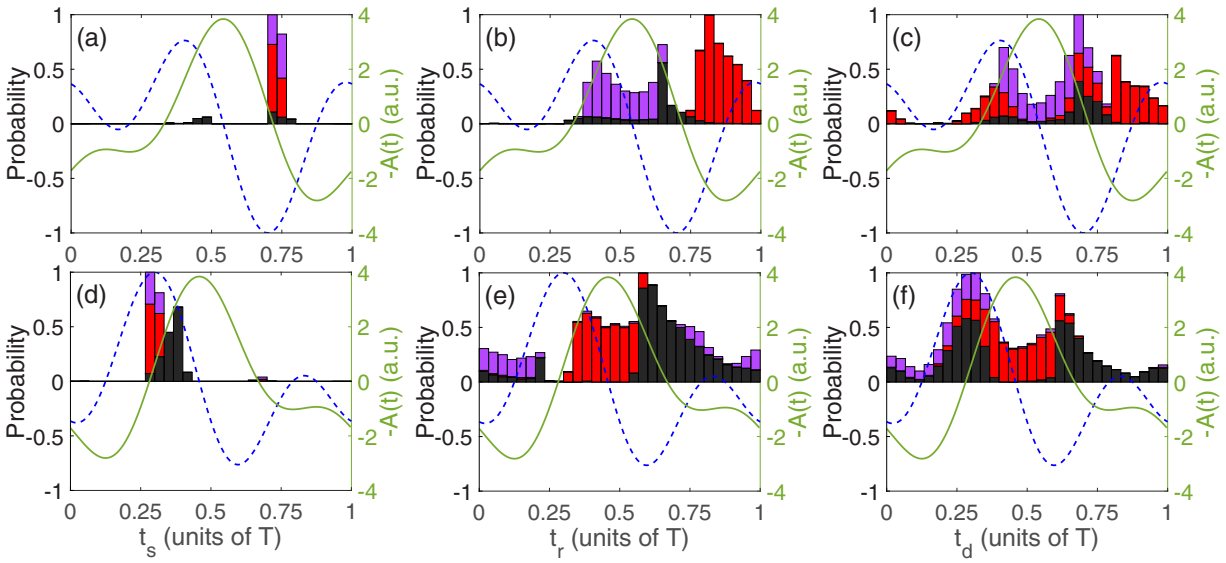

FIG. 3. The time distributions of (a) and (d) the single ionization, (b) and (e) recollision, and (c) and (f) double ionization for relative phases of 0.75π (top row) and 1.25π (bottom row). Black bars: FRR events; purple bars: ORR events without the FRR; and red bars: ERR events. The dashed and solid lines show the laser electric field and negative vector potential in arbitrary units.

NSDI induced by FRR trajectories is very small, and NSDI mainly proceeds by ORR trajectories and ERR trajectories [see Fig. 2(b) and the top row of Fig. 3]. The peaks in the negative and positive parts of the ion momentum distribution originate from ORR and ERR trajectories, respectively [see Fig. 2(b)]. Trajectory analysis indicates that the single ionization mainly happens near the field peak of $t = 0.7T$, as shown in Fig. 3(a). For ORR events without the FRR, the recollision and double ionization both mainly occur in a time interval centered at $\sim 0.54T$, which results in a positive acceleration for the two electrons [see the purple bars in Figs. 3(b) and 3(c)]. Therefore, these ORR events without the FRR form the peak in the negative part of the ion momentum distribution [see the dotted purple curve in Fig. 2(b)]. For ERR events, the recollision occurs near the field zero of $t = 0.87T$ [see the red bars in Fig. 3(b)]. After recollision, about half of those events immediately cause double ionization [see the red bars in Fig. 3(c)], and the two electrons obtain a big negative acceleration, which leads to a big positive ion momentum. For the other ERR events, the second electrons are delayed and ionize at subsequent field peaks of $t = 0.4T$ and $0.7T$ [see the red bars in Fig. 3(c)]. In this situation, finally, the first electron has a negative momentum, and the momentum of the second electron approaches zero. Therefore, these ERR events lead to the peak in the positive part of the ion momentum distribution [see the dashed red curve in Fig. 2(b)].

For $\phi = 1.25\pi$, the correlated emission is still dominant. But compared to $\phi = 0.75\pi$ there are more anticorrelated emissions, and thus, more ions are located around $p_{z,\mathrm{ion}} = 0$. The total ion momentum spectrum shows a triple-hump structure [see the solid blue curve in Fig. 2(d)]. In this phase, all three types of trajectories make considerable contributions to NSDI. The two peaks in the negative part of the ion momentum distribution originate from FRR and ERR trajectories, and the peak in the positive part of the ion momentum distribution originates from ORR trajectories [see Fig. 2(d)]. For FRR events, single ionization mainly occurs after the field peak of $t = 0.3T$. The recollision occurs in the time interval $[0.55T, T]$ with a peak at $\sim 0.58T$. After the recollision the colliding electron remains free. It may obtain an acceleration of -1.7–2.7 a.u., peaking at 1.15 a.u. [see the black bars in Fig. 3(e)]. The second electron may be ionized in the time intervals $[0.55T, T]$ and $[0.15T, 0.38T]$. Correspondingly, the acceleration of the second electron by the subsequent electric field is -1.7–2.7 a.u., peaking at 1.15 a.u., and -2.75–3 a.u., peaking at 0 a.u. Therefore, the final ion momentum shows a wide distribution from -5.7 to 4 a.u., with a peak located at 2.45 a.u. [see the dash-dotted black curve in Fig. 2(d)]. For the ORR events without the FRR, single ionization occurs near $t = 0.3T$, and the recollision happens in the time intervals $[0.75T, T]$ and $[0, 0.2T]$. Finally, the colliding electron obtains a negative acceleration. The second electron is mainly ionized in the time interval $[0, 0.35T]$ and therefore finally mainly obtains a negative acceleration [see the purple bars in Figs. 3(e) and 3(f)]. In this case both electrons are emitted in the negative direction, and thus, the ion is emitted in the positive direction. The ion momentum distribution shows a peak in the positive direction [see the dotted purple curve in Fig. 2(d)]. For the ERR events, single ionization occurs near $t = 0.3T$, and the recollision happens near the field zero of $t = 0.46T$. After the recollision, the colliding electron can obtain a big positive acceleration from the electric field. The second electron is mainly emitted in the time interval $[0.25, 0.6T]$ and finally drifts in the positive direction. Therefore, the momentum distribution of ions from ERR events shows a peak in the negative part [see the dashed red curve in Fig. 2(d)].

If we ignore the effect of the Coulomb potential, the final momentum of the second electron is equal to the negative vector potential at the double-ionization instant. When the recolliding electron returns with a high energy and forward scatters from the parent ion, the final momentum of the recolliding electron is approximately equal to the negative vector potential at the single-ionization instant. Therefore, the ion momentum is approximately equal to the sum of the vector

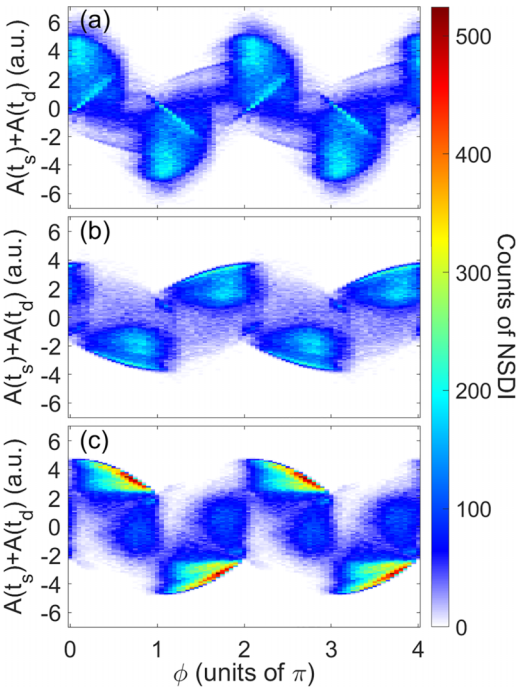

FIG. 4. The sum of the vector potentials at a single-ionization instant and a double-ionization instant vs the relative phase. (a) FRR events, (b) ORR events without the FRR, and (c) ERR events.

potentials at the single- and double-ionization instants. Figure 4 shows the sum of the vector potentials at the single- and double-ionization instants vs the relative phase for FRR events [Fig. 4(a)], ORR events without the FRR [Fig. 4(b)], and ERR events [Fig. 4(c)]. One can see that the shapes and trends with the relative phase of these distributions are basically the same as the ion momentum distributions in Figs. 1(b)–1(d). For example, for ERR events, in the relative phase 0–π, the sum of the vector potentials at single- and double-ionization instants and the ion momentum both show a narrow distribution, and their values decrease with the increase of the relative phase of the two pulses [see Figs. 1(d) and 4(c)]. Moreover, the magnitude of the ion momentum is approximately equal to that of the sum of the vector potentials. However, for FRR events, as shown in Figs. 1(b) and 4(a), the shapes and trends with the relative phase of the distribution from the sum of the vector potentials are basically the same as the ion momentum distribution, but the magnitude of the sum of the vector potentials is larger than that of the ion momentum. This is because in the approximation above used to obtain Fig. 4, the change in the momentum of the colliding electron during recollision is ignored and its final momentum is approximated by the negative vector potential at the single-ionization instant. This approximation is good for a forward-scattering electron with a high energy, whose momentum changes slightly during the recollision. But the approximation becomes bad for a forward-scattering electron with a low energy or a backward-scattering electron, whose momentum changes significantly during the recollision. Back analysis of NSDI trajectories indicates that there are more recolliding electrons with low energy for FRR events than for the other two types of trajectories. Therefore, the difference between the magnitude of the sum of the vector

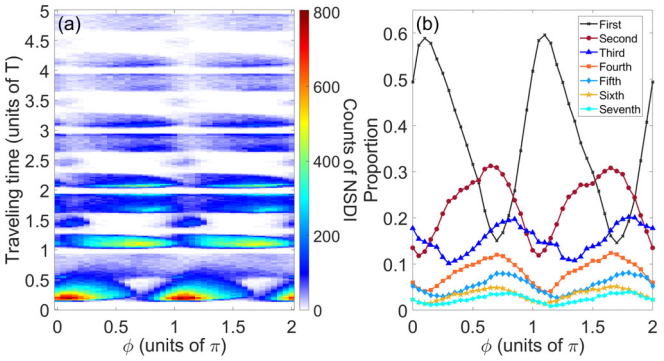

FIG. 5. (a) The traveling time vs the relative phase. (b) The proportion of the trajectories with different returning numbers in NSDI vs the relative phase.

potentials and the ion momentum for FRR events is more pronounced than for the other two types of trajectories.

The traveling time between single ionization and the recollision as a function of the relative phase of the two pulses is shown in Fig. 5(a). The traveling times show a series of separated values, which correspond to different returning numbers before recollision. As shown in Fig. 5(a), for a given phase, the contributions of trajectories with different returning numbers to NSDI are significantly different. Moreover, the contributions of trajectories with a certain returning number to NSDI are strongly dependent on the relative phase of the two pulses, as shown in Fig. 5(b). For example, the proportion of the FRR events in NSDI achieves its maximum of 59% at $\phi = 0.1\pi$ and minimum of 15% at $\phi = 0.7\pi$. This indicates that in the PPTC field with equal intensities the returning number can be controlled by changing the relative phase of the two pulses. In addition, we find that only in the phase ranges of $[0, 0.25\pi]$ and $[\pi, 1.25\pi]$ does the proportion of the FRR events in NSDI exceed 50%. This means that only in these two phase intervals are FRR events dominant, while for other phases NSDI mainly proceeds by multiple-returning trajectories in the PPTC field with equal intensities.

Finally, we discuss the NSDI mechanism in the PPTC field with equal intensities and its dependence on the relative phase of the two pulses and the returning numbers. After the recollision the first electron is ionized quickly. The second

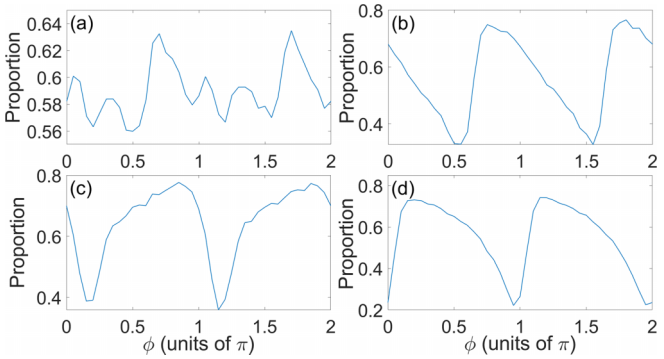

FIG. 6. The proportion of the RDI mechanism vs the relative phase for (a) all NSDI events, (b) the FRR events, (c) the ORR events without the FRR, and (d) the ERR events.

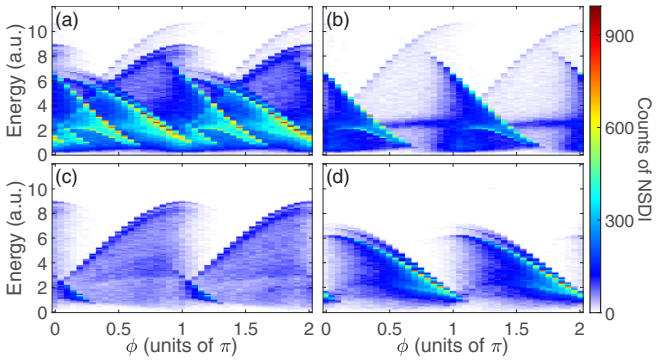

FIG. 7. The distributions of returning energy vs the relative phase for (a) all NSDI events, (b) the FRR events, (c) the ORR events without the FRR, and (d) the ERR events.

electron may be ionized quickly or may be promoted to an excited state and then released by the laser field at a later time. The two pathways are referred to as recollision direct ionization (RDI) and recollision excitation with subsequent field ionization (RESI). In our calculation, we define RDI (RESI) as the ionization mechanism when the delay time between the double ionization and the recollision is less than $T/8$ (more than $T/8$). Figure 6 shows the proportion of the RDI mechanism as a function of the relative phase for all NSDI events [Fig. 6(a)], the FRR events [Fig. 6(b)], the ORR events without the FRR [Fig. 6(c)], and the ERR events [Fig. 6(d)]. We can see that the proportion of the RDI mechanism varies periodically with the relative phase of the two pulses. For FRR events, in the phase range $[0.5\pi, 1.5\pi]$, the proportion of the RDI mechanism first abruptly rises and then linearly decreases. For ORR events without the FRR, in the phase range $[0.1\pi, 1.1\pi]$, the proportion of the RDI mechanism first slowly rises and then abruptly decreases. For ERR events in the phase range $[0, \pi]$, the proportion of the RDI mechanism first abruptly rises and then slowly decreases. Overall, the curves of the proportion of the RDI mechanism all oscillate around 0.5 for the three types of trajectories, as shown in Figs. 6(b)–6(d). This means that the dominant ionization mechanism changes with the relative phase of the two pulses. In the PPTC field with equal intensities, by changing the relative phase of the two pulses the dominant ionization mechanism can be well controlled for the three types of trajectories.

To clarify the reason for the dependence of the NSDI mechanism on the relative phase of the two pulses, we analyze the returning energy of the ionized electron, as shown in Fig. 7. Here, we define the energy of the returning electron (including the kinetic energy, the potential energy of the electron-ion interaction, and half of the electron-electron repulsion) as the returning energy when two electrons are 2.5 a.u. apart before the recollision. We can see that the returning energy can be well controlled by changing the relative phase in the PPTC fields with equal intensities. By comparing Figs. 6 and 7, we can see that the variation trend of the returning energy of the ionized electron with the relative phase is consistent with the change trend of the proportion of the RDI mechanism. For example, for ERR events, in Fig. 7(d), when the relative phase increases from 0 to π, the returning energy abruptly jumps from 1.5 to 6 a.u., resulting in a sharp increase of the proportion of the RDI mechanism, and then the returning energy slowly decreases, leading to a slow decrease of the proportion of the RDI mechanism [see Fig. 6(d)]. These results indicate that one can control the returning energy of the ionized electron and further manipulate the NSDI mechanism in the PPTC field by changing the relative phase of the two pulses.

IV. SUMMARY

In conclusion, we investigated NSDI of He in a PPTC field with equal intensities using a three-dimensional classical ensemble model. The ion momentum distribution shows pronounced asymmetry and strongly depends on the relative phase of the two pulses. The ion momentum distributions exhibit a double- or triple-hump structure, depending on the relative phase of the two pulses. The triple-hump structure was not observed in previous studies using a PPTC field with two significantly different intensities. Moreover, different from the PPTC field with two significantly different intensities, where the recollision occurs at the first returning of the free electron, the multiple-returning recollision trajectories make a considerable contribution to NSDI, and its proportion in NSDI depends on the relative phase of the two pulses. The three peaks of the ion momentum distribution correspond to the FRR trajectories, the ORR trajectories without the FRR, and the ERR trajectories. This means that the electron returning dynamics in NSDI by PPTC fields leaves a footprint in the ion momentum distribution. Moreover, with the variation of the relative phase, the contribution of FRR trajectories to NSDI periodically changes. It reaches the maximum at $\phi = 0.1\pi$ and the minimum at $\phi = 0.7\pi$. Back analysis showed that the returning energy of the ionized electron strongly depends on the relative phase of the two pulses. The contributions of the RDI and RESI mechanisms to NSDI can be controlled by changing the relative phase. This provides an avenue to directly obtain information about electron returning dynamics from the ion momentum spectra and to control the subcycle dynamics of the recollision process.

ACKNOWLEDGMENTS

This work was supported by the National Natural Science Foundation of China under Grants No. 12074329 and No. 12004323.

[1] D. N. Fittinghoff, P. R. Bolton, B. Chang, and K. C. Kulander, Phys. Rev. Lett. **69**, 2642 (1992).

[2] B. Walker, B. Sheehy, L. F. DiMauro, P. Agostini, K. J. Schafer, and K. C. Kulander, Phys. Rev. Lett. **73**, 1227 (1994).

[3] C. Figueira de Morisson Faria and X. Liu, J. Mod. Opt. **58**, 1076 (2011).

[4] W. Becker, X. J. Liu, P. J. Ho, and J. H. Eberly, Rev. Mod. Phys. **84**, 1011 (2012).

[5] Th. Weber, H. Giessen, M. Weckenbrock, G. Urbasch, A. Staudte, L. Spielberger, O. Jagutzki, V. Mergel, M. Vollmer, and R. Dörner, Nature (London) **405**, 658 (2000).

[6] M. Lein, E. K. U. Gross, and V. Engel, Phys. Rev. Lett. **85**, 4707 (2000).

[7] J. S. Parker, B. J. S. Doherty, K. T. Taylor, K. D. Schultz, C. I. Blaga, and L. F. DiMauro, Phys. Rev. Lett. **96**, 133001 (2006).

[8] X. Wang and J. H. Eberly, Phys. Rev. Lett. **105**, 083001 (2010).

[9] F. Mauger, C. Chandre, and T. Uzer, Phys. Rev. Lett. **102**, 173002 (2009).

[10] X. L. Hao, J. Chen, W. D. Li, B. Wang, X. Wang, and W. Becker, Phys. Rev. Lett. **112**, 073002 (2014).

[11] D. Ye, M. Li, L. Fu, J. Liu, Q. Gong, Y. Liu, and J. Ullrich, Phys. Rev. Lett. **115**, 123001 (2015).

[12] X. Chen, C. Ruiz, F. He, and J. Zhang, Opt. Express **28**, 14884 (2020).

[13] J. L. Chaloupka and D. D. Hickstein, Phys. Rev. Lett. **116**, 143005 (2016).

[14] C. A. Mancuso, K. M. Dorney, D. D. Hickstein, J. L. Chaloupka, J. L. Ellis, F. J. Dollar, R. Knut, P. Grychtol, D. Zusin, C. Gentry, M. Gopalakrishnan, H. C. Kapteyn, and M. M. Murnane, Phys. Rev. Lett. **117**, 133201 (2016).

[15] S. Eckart, M. Richter, M. Kunitski, A. Hartung, J. Rist, K. Henrichs, N. Schlott, H. Kang, T. Bauer, H. Sann, L. Ph. H. Schmidt, M. Schöffler, T. Jahnke, and R. Dörner, Phys. Rev. Lett. **117**, 133202 (2016).

[16] P. B. Corkum, Phys. Rev. Lett. **71**, 1994 (1993).

[17] K. C. Kulander, J. Cooper, and K. J. Schafer, Phys. Rev. A **51**, 561 (1995).

[18] B. Feuerstein, R. Moshammer, D. Fischer, A. Dorn, C. D. Schröter, J. Deipenwisch, J. R. Crespo Lopez-Urrutia, C. Höhr, P. Neumayer, J. Ullrich, H. Rottke, C. Trump, M. Wittmann, G. Korn, and W. Sandner, Phys. Rev. Lett. **87**, 043003 (2001).

[19] Y. Liu, L. Fu, D. Ye, J. Liu, M. Li, C. Wu, Q. Gong, R. Moshammer, and J. Ullrich, Phys. Rev. Lett. **112**, 013003 (2014).

[20] Q. Liao, A. H. Winney, S. K. Lee, Y. F. Lin, P. Adhikari, and W. Li, Phys. Rev. A **96**, 023401 (2017).

[21] A. S. Maxwell and C. Figueira de Morisson Faria, Phys. Rev. Lett. **116**, 143001 (2016).

[22] Y. Liu, S. Tschuch, A. Rudenko, M. Durr, M. Siegel, U. Morgner, R. Moshammer, and J. Ullrich, Phys. Rev. Lett. **101**, 053001 (2008).

[23] A. Staudte, C. Ruiz, M. Schöffler, S. Schössler, D. Zeidler, Th. Weber, M. Meckel, D. M. Villeneuve, P. B. Corkum, A. Becker, and R. Dörner, Phys. Rev. Lett. **99**, 263002 (2007).

[24] A. Rudenko, V. L. B. de Jesus, Th. Ergler, K. Zrost, B. Feuerstein, C. D. Schröter, R. Moshammer, and J. Ullrich, Phys. Rev. Lett. **99**, 263003 (2007).

[25] A. Emmanouilidou, Phys. Rev. A **78**, 023411 (2008).

[26] D. F. Ye, X. Liu, and J. Liu, Phys. Rev. Lett. **101**, 233003 (2008).

[27] Y. Zhou, Q. Liao, and P. Lu, Phys. Rev. A **82**, 053402 (2010).

[28] Z. Chen, Y. Liang, and C. D. Lin, Phys. Rev. Lett. **104**, 253201 (2010).

[29] B. Wolter, M. G. Pullen, M. Baudisch, M. Sclafani, M. Hemmer, A. Senftleben, C. D. Schröter, J. Ullrich, R. Moshammer, and J. Biegert, Phys. Rev. X **5**, 021034 (2015).

[30] C. Huang, M. Zhong, and Z. Wu, Opt. Express **24**, 28361 (2016).

[31] T. Shaaran, N. Camus, J. Dura, L. Fechner, A. Thai, A. Britz, M. Baudisch, T. Steinle, A. Senftleben, C. D. Schröter, J. Ullrich, T. Pfeifer, C. H. Keitel, J. Biegert, K. Z. Hatsagortsyan, and R. Moshammer, Phys. Rev. A **99**, 023421 (2019).

[32] Y. Li, X. Wang, B. Yu, Q. Tang, G. Wang, and J. Wan, Sci. Rep. **6**, 37413 (2016).

[33] Y. L. Wang, S. P. Xu, W. Quan, C. Gong, X. Y. Lai, S. L. Hu, M. Q. Liu, J. Chen, and X. J. Liu, Phys. Rev. A **94**, 053412 (2016).

[34] X. Liu, H. Rottke, E. Eremina, W. Sandner, E. Goulielmakis, K. O. Keeffe, M. Lezius, F. Krausz, F. Lindner, M. G. Schätzel, G. G. Paulus, and H. Walther, Phys. Rev. Lett. **93**, 263001 (2004).

[35] B. Bergues, M. Kübel, N. G. Johnson, B. Fischer, N. Camus, K. J. Betsch, O. Herrwerth, A. Senftleben, A. M. Sayler, T. Rathje, T. Pfeifer, I. Ben-Itzhak, R. R. Jones, G. G. Paulus, F. Krausz, R. Moshammer, J. Ullrich, and M. F. Kling, Nat. Commun. **3**, 813 (2012).

[36] N. Camus, B. Fischer, M. Kremer, V. Sharma, A. Rudenko, B. Bergues, M. Kubel, N. G. Johnson, M. F. Kling, T. Pfeifer, J. Ullrich, and R. Moshammer, Phys. Rev. Lett. **108**, 073003 (2012).

[37] C. Huang, W. Guo, Y. Zhou, and Z. Wu, Phys. Rev. A **93**, 013416 (2016).

[38] G. G. Paulus, W. Becker, and H. Walther, Phys. Rev. A **52**, 4043 (1995).

[39] X. Xie, S. Roither, D. Kartashov, E. Persson, D. G. Arbo, L. Zhang, S. Gräfe, M. S. Schöffler, J. Burgdörfer, A. Baltuska, and M. Kitzler, Phys. Rev. Lett. **108**, 193004 (2012)

[40] S. Luo, M. Li, H. Xie, P. Zhang, S. Xu, Y. Li, Y. Zhou, P. Lan, and P. Lu, Phys. Rev. A **96**, 023417 (2017).

[41] J. Liang, Y. Zhou, Y. Liao, W. Jiang, M. Li, and P. Lu, Ultrafast Sci. **2022**, 9842716 (2022).

[42] Y. Zhou, Q. Liao, Q. Zhang, W. Hong, and P. Lu, Opt. Express **18**, 632 (2010).

[43] X. Ma, Y. Zhou, and P. Lu, Opt. Laser Technol. **108**, 235 (2018).

[44] S. Luo, X. Ma, H. Xie, M. Li, Y. Zhou, W. Cao, and P. Lu, Opt. Express **26**, 13666 (2018).

[45] S. L. Haan, L. Breen, A. Karim, and J. H. Eberly, Phys. Rev. Lett. **97**, 103008 (2006).

[46] T. Xu, Q. Zhu, J. Chen, S. Ben, J. Zhang, and X. Liu, Opt. Express **26**, 1645 (2018).

[47] B. Li, X. Yang, X. Ren, and J. Zhang, Opt. Express **27**, 32700 (2019).

[48] C. Huang, H. Pang, X. Huang, M. Zhong, and Z. Wu, Opt. Express **28**, 10505 (2020).